Antimonide-based Superlattice Infrared Barrier Photodetectors

U. Zavala-Moran[1], R. Alchaar[2], J. P. Perez[2], J. B. Rodriguez[2], M. Bouschet[2], V. H. Compean[1],
F. de Anda[1] and P. Christol[2]

[1]*IICO, UASLP, San Luis Potosí, Mexico*
[2]*IES, Univ. Montpellier, CNRS, Montpellier, France*

Abstract: Barrier structures are now the design of high performance antimonide-based (Sb-based) cooled infrared (IR) quantum detectors. In this communication, we report on electrical and electro-optical characterizations of Ga-free and Ga-containing type-II superlattices (T2SL) photodetectors structures grown by Molecular Beam Epitaxy (MBE). Experimental measurements on Ga-free XBn and Ga-containing XBp samples were made by photo-response measurements and dark current density-voltage (J-V) characteristics performed on detectors as a function of temperature. Identification of bias voltage characteristics were extracted from measurements and resulting dark current values were compared to the state of the art of infrared technology.

1   INTRODUCTION

In order to reduce the dark current, and therefore the noise of the device, the first infrared (IR) barrier detector was proposed by A. White in 1983 (White, 1983). He proposed an architecture device composed of isotype (n-type) heterostructures where a high band gap energy barrier layer was placed between the absorbing and contact layers of smaller gap materials. As the objective of the barrier layer is to block the majority carriers (in this case electrons) while allowing the photogenerated minority carriers (holes) to reach the contact layer, he called this device "high impedance photoconductor". However, at that time, obtaining a very low or zero valence band offset was difficult to achieve with the main IR detection materials based on InSb and HgCdTe (MCT). Everything changed in the mid-2000s with the demonstration of the InAs-based barrier structure by Maimon and Wicks (Maimon, 2006) and then accelerated with the used of antimonide-based (Sb-based) materials, such as InAsSb (Klipstein, 2011) and type II superlattice (T2SL) structures lattice matched to GaSb substrate (Klipstein, 2015), to build IR barrier photodetectors.

Barrier structures are now the standard for the design of Sb-based cooled IR photodetectors. Such high-performance detector structure, which replaced the usual pin photodiode, is made of n-type or p-type photon absorbing layer, a barrier layer B and a contact layer X that can be made from either the same, or a different material, to that used for the photon absorbing layer. Consequently, these quantum detectors are named XBn or XBp structures, also called bariodes.

Specialist of IR photonic Sb-based devices fabricated by Molecular Beam Epitaxy (MBE) on GaSb substrate, the Institute of Electronic and Systems (IES) of the University of Montpellier (France) has studied T2SL quantum detectors dedicated to IR spectral domain since several years (Rodriguez, 2005, Jaworowicz, 2010, Delmas, 2014). This paper reports electro-optical and electrical experimental measurements performed on Ga-free InAs/InAsSb and Ga-containing InAs/GaSb T2SL structures, grown by MBE, in XBn and XBp photodetector configurations, respectively.

2   T2SL XBN AND T2SL XBP BARRIER STRUCTURES

2.1   Advantages of Barrier Structure

To understand the advantages of the barrier detector, is necessary to compare it with the pn junction photodiode.

In the pn junction structure with reverse bias applied, the presence of the space charge zone on either side of the p/n interface blocks the transport of

the majority carriers and allows the transfer of the minority ones. However, this zone with electric field generates Shockley-Read-Hall (SRH) recombination darkness current, thus generation-recombination (GR) current, which may be important in the IR spectral domain. Dark current of IR photodiodes, such as InSb, is dominated by SRH current at its operating temperature (~80K).

The main objective of the XBn or XBp barrier structure is to reduce the contribution of the SRH current to the dark current of the detector. For that, it is required to control the electric field zone by confining it in the high band gap barrier material instead of in the absorbing zone structure. Then, SRH processes occur in the high band gap material, not in the IR absorbing layer. In addition, the barrier layer plays the same role as the space charge zone in the pn structure as blocking the majority carriers and allowing the flow of the minority ones.

Consequently, when the barrier detector structure is correctly designed, GR dark current is strongly reduced, even eliminated, and the performances of the photodetector are improved (Klipstein, 2015).

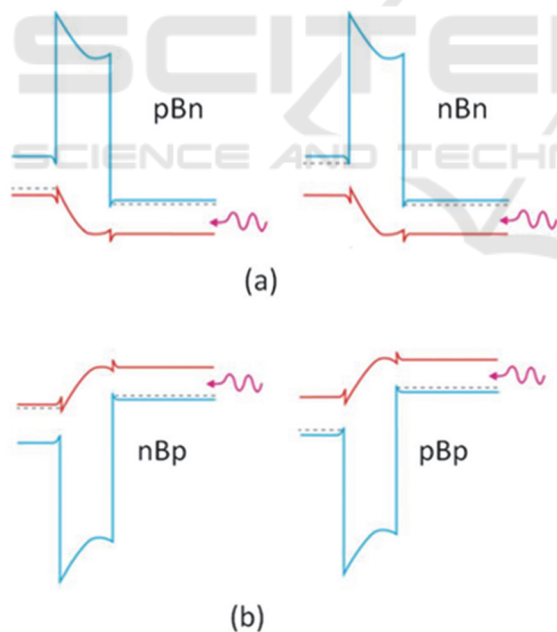Figure 1 shows the possible XBn and XBp designs.

(a)

(b)

Figure 1: Schematic view of XBn (a) and XBp (b) structures. In each case, the contact layer (X) is on the left and the IR absorbing layer (n or p) is on the right (according to (Klipstein, 2015)).

2.2 T2SL Structures

The type-II superlattice (T2SL) was proposed at the end of the 80's as a material for IR detection (Smith, 1987).

A superlattice is a stack of periodic layers whose thickness is of the order of a few nanometers. It is an artificial quantum structure composed of coupled multi-quantum wells. Carriers (electrons and holes) are then confined into energy minibands and optical absorption occurs between two of these minibands.

In the case of Sb-based materials, such quantum structure presents particular type-II band alignment where the carriers are confined in the adjacent materials (Figure 2) and, depending on the thickness layers, the fundamental valence to conduction (V1-C1) interminiband absorption (detector cut-off wavelength λ_c) can address all the thermal IR, from 3 to 30µm (Wei, 2004).

Figure 2 shows a Ga-containing InAs/GaSb T2SL fundamental absorption spectrum at T= 300K.
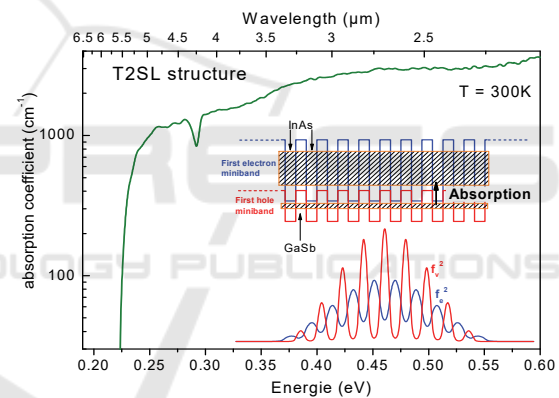

Figure 2: T2SL absorption coefficient extracted from room temperature absorption spectrum. In the inset, band diagram and probability densities of fundamental C1 and V1 levels of first electron and heavy hole (hh) minibands are reported.

3 T2SL XBN AND T2SL XBP DETECTORS: FABRICATION AND CHARACTERIZATION

Lattice-matched to the GaSb substrate, the absorbing zone is composed of strain compensated Ga-free InAs/InAsSb or Ga-containing InAs/GaSb T2SL, operating in the MWIR (midwave infrared 3-5µm) to LWIR (longwave infrared 8-12µm) spectral domains, respectively.

3.1 Ga-free T2SL XBn Photodetector

The XBn detector operating in the MWIR domain is made of 1μm-thick non-intentionally doped (nid) n-type Ga-free $InAs/InAs_{0.69}Sb_{0.31}$ T2SL absorbing layer, 80nm-thick p-doped $AlAs_{0.09}Sb_{0.91}$ barrier layer and 100nm-thick n^+-doped $InAs/InAs_{0.69}Sb_{0.31}$ T2SL contact layer (Figure 3). Equivalent Ga-free structure has recently been fabricated on Si substrate (Durlin, 2019)
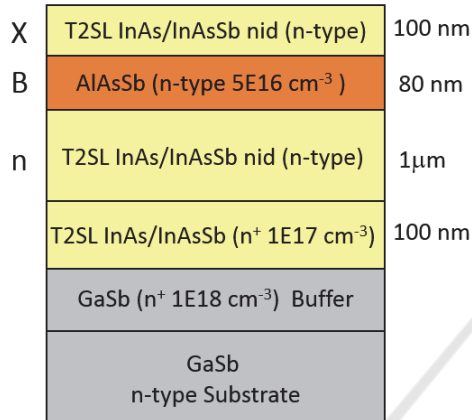

Figure 3: Schematic cross-section of the Ga-free T2SL XBn photodetector on GaSb substrate.

Figure 4 displays the high-resolution x-ray diffraction (HRXRD) spectrum of the T2SL XBn structure grown by MBE on 2" (100) GaSb substrate. The presence of numerous and intense satellite peaks is a signature of the crystallographic structure's quality and their positions allow to calculate the InAs/InAsSb period thickness of the T2SL stacking equal to 4.40 nm.
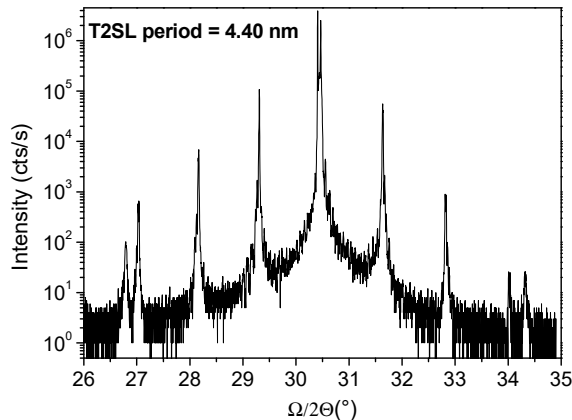

Figure 4: High-resolution X-ray diffraction patterns of Ga-free T2SL InAs (3.30nm)/$InAs_{0.69}Sb_{0.31}$ (1.10nm) structure on GaSb substrate.

From epitaxial SL material, circular mesa photodiodes were fabricated using standard photolithography with a mask set containing diodes and photodiodes with several diameters, from 60μm up to 310μm (figure 5). Mesa photodiodes were realized by wet etching using citric acid solution and polymerized photoresist was used to protect the mesa surface from ambient air. Metallization were ensured on the n-GaSb substrate and on the n-type T2SL cap layer. Next, the devices are mounted in a cryogenic probe station to perform dark current density-voltage (J-V) measurements.
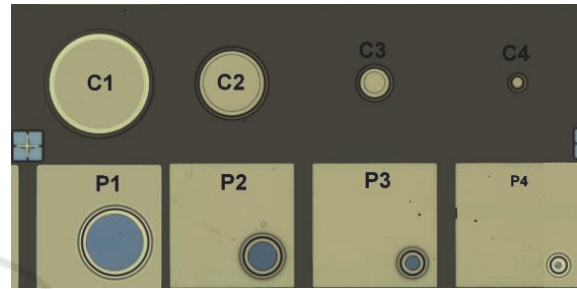

Figure 5: Top view of a processed sample, blind diodes (C) and photodiodes (P) with several diameters from 60μm up to 310μm.

Figure 6 shows the J-V curves at temperatures ranging from 77 to 250K, performed on a detector with a 210 μm-diameter. At low temperature, until 110K, the dark current is limited by the photonic current due to the experimental set-up (probe station).

The shapes of the dark J(V) characteristics are in accordance with the those obtained with XBn Ga-free MWIR diodes, reported elsewhere (Baril, 2016 ; Ting, 2018).
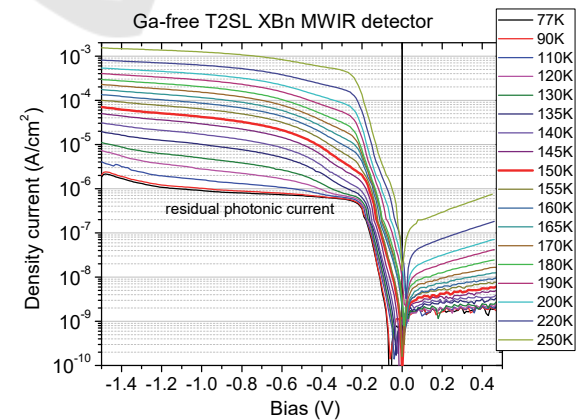

Figure 6: Dark current density-voltage (J-V) characteristics at different temperatures, from 77 to 250K, of a Ga-free T2SL XBn MWIR detector.

In the forward positive bias, the low dark current is due to the thin n-type top contact layer compared to the absorbing layer (100 nm vs 1µm). A slight negative bias applied to the top contact layer (typically - 200mV) is necessary for the device operation.

At temperature lower than 180K, the slope of the dark currents plots between -0.1V and -0.4V shows the presence of GR current, indicating that the device design must be optimised. At higher temperature, one can see that the slope is reduced as diffusion current becomes dominant in the dark current.

At the expected operation temperature equal to 150K, dark current density as low as 2×10^{-6} A/cm^2, at typical bias operation equal to -200mV, is extracted. Lower dark current could be obtained by a better control of targeted doping values of MBE grown layers.

The samples were then wire bounded onto a 68 pin LCC and placed in a liquid nitrogen cryostat in order to perform non-calibrated photoresponse (PR) measurements by using a Nicolet-870 Nexus Fourier transform infrared (FTIR) spectrometer with non-calibrated IR source. Figure 7 shows the front side illuminated uncalibrated PR spectra obtained at different biases and at T = 150K. One can observe a 50% cut-off wavelength at 4.2µm and that the collected signal begins to saturate at bias applied equal to -220mV.
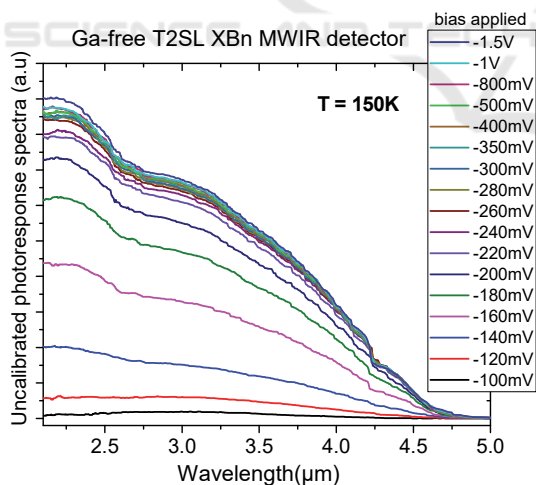

Figure 7: Uncalibrated PR spectra recorded at T= 150K, for different biases applied from -100 to 1500mV, of a Ga-free T2SL XBn MWIR detector.

To explain the behaviour of the PR spectrum as a function of bias applied, band diagrams of the XBn device are calculated at T= 150K and reported in
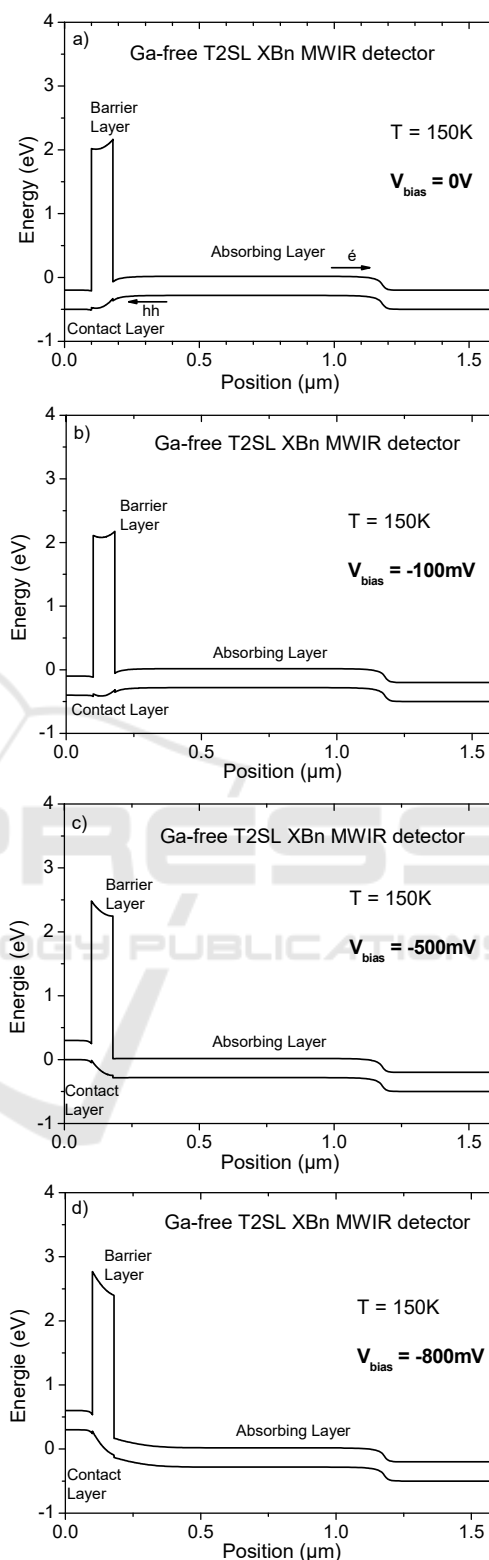

Figure 8: Calculated band diagrams using the ATLAS software from SILVACO (Abautret, 2013) of the Ga-free XBn barrier structure at 150K and 0V (a), -100mV (b), -500mV (c), and -800mV (d).

48

Figure 8 for four typical bias voltages ($V_{bias} = 0V$, $V_{bias} = -100mV$, $V_{bias} = -500mV$, $V_{bias} = -800mV$).

At $V_{bias} = 0V$, the band diagram highlights the presence of a potential barrier blocking the minority heavy hole carriers. Even, at bias operation equal to -100mV, this potential barrier remains, penalizing the quantum efficiency (Figure 7).

At $V_{bias} = -500mV$, the bias is high enough to suppress the potential barrier allowing the transport of hole minority carrier to the top contact layer. The maximum of PR is collected.

3.2 Ga-containing T2SL XBp photodetector

In this part, another kind of barrier structure is considered. It is a Ga-containing InAs/GaSb T2SL XBp detector operating in the LWIR domain.

To maximize the quantum efficiency, the Ga-containing T2SL is p-type doping (Giard, 2014). Consequently, the electrons are the minority carriers and the barrier, made of InAs/AlSb T2SL (Delmas, 2017), is tailored to have a large offset in the valence band and minimal offset in the conduction band, therefore blocking majority holes and collecting photo-generated electrons.

The XBp detector structure under consideration is made of lightly p-type doped 3.2µm thick InAs/GaSb T2SL absorbing layer, a heavily n-type doped wide bandgap InAs/GaSb T2SL and a lightly n-type doped InAs/AlSb barrier layer. Figure 9 shows the calculated band diagram at 80K and under no bias.
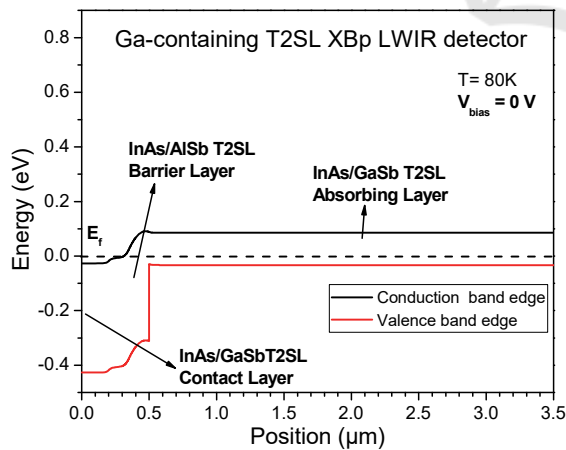

Figure 9: Calculated band diagram of the Ga-containing XBp barrier structure at 80K and 0V.

In addition of the photoluminescence (PL) spectrum, figure 9 displays the non-calibrated photo-response (PR) spectrum at $V_{bias} = -100mV$ for a detector device having a 90 µm-diameter. The 50%

cut-off wavelength equal to 10.5µm for the spectral PR corresponds to the PL peak, in agreement with the targeted value suitable for LWIR applications. The inset shows the PR measurements at different biases and the PR starts to saturate after -50mV bias applied, enough to reduce the possible conduction potential barrier (Figure 9). Measured elsewhere (Höglund, 2018), the detector quantum efficiency (without anti-reflection coating) reaches 35% at 80K. Figure 11a reports normalized PR values extracted from the PR measurements (inset Figure 11) at different biases and at 10.5µm.

Dark current density-voltage measurement (J-V) is also performed at 80K. J_{dark} result is shown in Figure 11b and the associated differential resistance area product R_dA is reported in Figure 11c (R_d is calculated from the derivative of the voltage over the current and A is the device area).
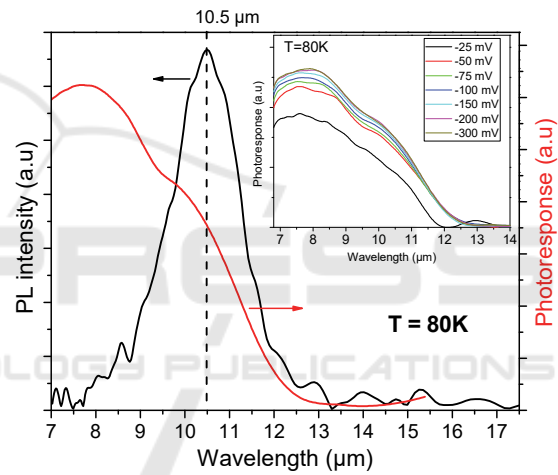

Figure 10: PL and PR (at $V_{bias} = -100mV$) measurements at 80K of a Ga-containing XBp T2SL detector device. The inset shows the PR at different biases.

The shape of the curves displayed in Figure 11, help us to identify the two main dark current regimes of the LWIR detector. First, the operating bias $V_{op} = -100mV$. At this bias, the device is fully turned on (where R_dA is at a maximum value), the diffusion plateau is reached, and the PR value saturates. The depletion region is still confined within the barrier. Next, the $V_{GR} = -300$ mV. At this bias, GR current starts to dominate the dark current of the diode, the barrier is fully depleted, and the depletion region reaches the absorbing region.

From this analysis, it is possible to identify the operating bias of the device, which is -100mV. At this voltage, dark current density value as low as 8×10^{-4} A/cm^2 and R_dA product as high as 1160 Ω.cm^2 are extracted at T = 80K.
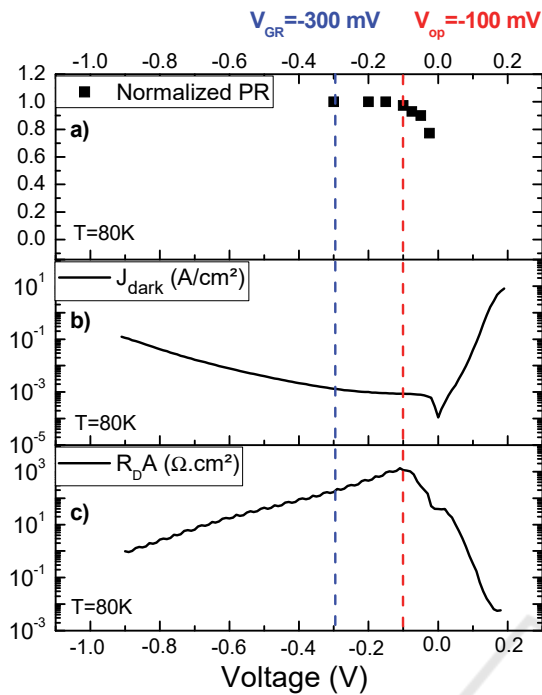
Figure 11: Experimental characterizations of a Ga-containing XBp T2SL detector device. From top to bottom : (a) normalized PR, (b) dark current density J_{dark}, (c) differential resistance area product (R_dA) as a function of the voltage at T = 80K. Two particular bias are identified : The operating bias V_{op} and the V_{GR} bias for which the G-R current begins to dominate the dark current of the diode.

4 CONCLUSIONS

InAs/InAsSb Ga-free XBn T2SL MWIR and InAs/GaSb Ga-containing XBp T2SL LWIR quantum detectors have been fabricated and characterized.

These photodetectors showed cut-off wavelength around 4.2µm at 150K and 10.5µm at 80K, respectively. Dark current density values, extracted from J(V) measurements, are equal to 2×10^{-6} A/cm² at 150K for the Ga-free device and 8×10^{-4} A/cm² for the Ga-containing one.

Compared to the state of the art (i.e; the Rule 07 (Tennant, 2008)), these values are from two to one decades higher, respectively. Concerning the Ga-free T2SL, such result is due to the presence of GR dark current at operating bias. Improvement in the design and on the control of doping layers during the MBE growth are necessary to suppress this behaviour and will be the subject of forthcoming studies. For the Ga-containing T2SL, the origin of high dark current is different. The current of the device is dominated by

diffusion current at operating bias but the performance is penalized by the well-known poor lifetime value of minority carriers in Ga-containing T2SL (Svensson, 2011). A solution would be the development of Ga-free T2SL quantum detector structure dedicated for the LWIR spectral domain.

ACKNOWLEDGEMENTS

REFERENCES

Abautret, J., Perez, J.P., Evirgen, A., Martinez, F., Christol, P., Fleury, J., Sik, H., Cluzel, R., Ferron, A., Rothman, J., 2013. Electrical modeling of InSb PiN photodiode for avalanche operation, *Journal of Applied Physics,* 113, 183716.

Baril, N., Brown, A., Maloney, P., Tidrow, M., Lubyshev, D., Qui, Y., Fastenau, J.M., Amy W. K. Liu, A.W.K., Bandara, S., 2016. Bulk InAsSb nBn photodetectors with greater than 5lm cutoff on GaSb, *Applied Physics Letters*, 109, 122104

Delmas, M., Rodriguez, J.B., Christol, P., 2014. Electrical modeling of InAs/GaSb superlattice mid-wavelength infrared pin photodiode to analyze experimental dark current characteristics, *Journal of Applied Physics*, 116, 113101

Delmas, M., Rossignol, R., Rodriguez, J.B., Christol, P., 2017. Design of InAs/GaSb superlattice infrared barrier detectors, *Superlattices and Microstructures*, 104, 402.

Durlin, Q., Perez, J.P., Cerutti, L., Rodriguez, J.B., Cerba, T., Baron, T., Tournie, E., Christol, P., 2019. Midwave infrared barrier detector based on Ga-free InAs/InAsSb type-II superlattice grown by molecular beam epitaxy on Si substrate, *Infrared Physics & Technology* 96, 39

Giard, E., Ribet-Mohamed, I., Jaeck, J., Viale, T., Haïdar, R., Taalat, R., Delmas, M., Rodriguez, J.B., Steveler, E., Bardou, N., Boulard, F., Christol, P., 2014. Quantum efficiency investigations of type-II InAs/GaSb midwave infrared superlattice photodetectors, *Journal of Applied Physics,* 116, 043101.

Höglund, L., Rodriguez, J.B., Marcks von Würtemberg, M., Naureen, S., Ivanov, R., Asplund, C., Alchaar, R., Christol, P., Rouvié, A., Brocal, J., Saint-Pé, O., Costard, E., 2018. Influence of shallow versus deep etching on dark current and quantum efficiency in InAs/GaSb superlattice photodetectors and focal plane

arrays for long wavelength infrared detection, *Infrared Physics & Technology* 95, 158.

Jaworowicz, K., Ribet-Mohamed, I., Cervera, C., Rodriguez, J.B., Christol, P. 2010. Noise characterization of midwave infrared InAs/GaSb superlattice pin photodiode, *IEEE Photonics Technology Letters,* 23, 242

Klipstein, P., Klin, O., Grossman, S., Snapi, N., Lukomsky, I., Aronov, D., Yassen, M., Glozman, A., Fishman, T., Berkowicz, E., Magen, O., Shtrichman, I., Weiss, E., 2011. XBn barrier photodetectors based on InAsSb with high operating temperatures, *Optical Engineering,* 50, 061002

Klipstein, P., 2015. XBn and XBp infarred detectors, *Journal of Crystal Growth,* 425, 351.

Maimon, S., Wicks, G., 2006. nBn detector, an infrared detector with reduced dark current and higher operating temperature, *Applied Physics Letter,* 89, 151109.

Rodriguez, J.B., Christol, P., Ouvrard, A., Chevrier, F., Grech, P., Joullié, A. 2005. Uncooled InAs/GaSb superlattice photovoltaic detector operating in the mid-wavelength infrared range, *Electronics Letters,* 41, 362

Smith, D.L., Mailhiot, C., 1987. Proposal for strained type II superlattice infrared detectors, *Journal of Applied Physics,* 62, 2545.

Svensson, S.P., Donetsky, D., Wang, D., Hier, H., Crowne, F.J., Belenky, G., 2011. Growth of type II strained layer superlattice, bulk InAs and GaSb materials for minority lifetime characterization, *Journal of Crystal Growth*, 334, 103.

Tennant, W.E., Lee, D., Zandian, M., Piquette, E., Carmody, M., 2008. MBE HgCdTe Technology: A Very General Solution to IR Detection, Described by ''Rule 07'', a Very Convenient Heuristic, *Journal of Electronic Materials*, 37, 1406

Ting, D. Z., Soibel, A., Khoshakhlagh, A., Rafol, S.B., Keo, S.A., Höglund, L., Fisher, A.M., Luong, E.M., Gunapala, S.D., 2018. Mid-wavelength high operating temperature barrier infrared detector and focal plane array, Applied Physics Letters, 113, 021101

Wei, Y., Razeghi, M., 2004. Modeling of type-II InAs/GaSb superlattices using an empirical tight-binding method and interface engineering, *Physical Review B,* 69, 085316.

White, A., 1983. Infrared detectors, *US Patent,* 4 679 063.